# Experimental and Computational Demonstration of In Situ Pt Nanocluster-Decorated ZnO Film for Ultra-Sensitive Hydrogen Detection

Puja Ghosh[1], Pritam Ghosh[2], Rizwin Khanam[1], Chandra Shekhar Prajapati[3], Aarti Nagarajan[4], Shreeja Das[5], Rakesh Paleja[6], Sharan Shetty[5], Gopalakrishnan Sai Gautam[2], Navakanta Bhat[1, *]

[1]Centre for Nano Science and Engineering, Indian Institute of Science, Bengaluru 560012, India [2]Department of Materials Engineering, Indian Institute of Science, Bengaluru 560012, India, [3]Indian Institute of Technology Patna, Patna, Bihar 801106 [4]Shell Global Solutions (US) Inc., 3333 Highway 6 South, Houston, Texas 77082, United States [5]Shell India Markets Pvt., Ltd., Mahadeva Kodigehalli, Bengaluru 562149, Karnataka, India [6]Shell Research Limited, London, London Borough of Lambeth, SE1 7NA, United Kingdom.

*Corresponding author. E-mail address: navakant@iisc.ac.in; navakant@gmail.com

## S1. Materials and Methods:

### S1.1 Characterization of the Fabricated Films

The crystal structure, phases and structural properties of fabricated thin film were investigated by X-ray diffraction (Rigaku SMART Lab) using CuK$\alpha$ radiation ($\lambda$ = 1.54 A). X-ray photoelectron spectroscopy (XPS-Kratos Axis Ultra DLD) was used for quantitative elemental analysis of chemical composition and stoichiometry study of the film with monochromatic AlK$\alpha$ source (1486.6 eV). The surface structure, film uniformity and morphological analysis were done by using a Scanning Electron Microscope (FE-SEM; Ultra-55, Zeiss). The thickness measurement of the fabricated film was performed using an SEM cross-sectional measurement. Bruker Atomic Force Microscopy (AFM) was used to visualise the surface topography of the sample to characterise the surface roughness, step heights and molecular structures. The work function of the fabricated material was measured by Kelvin Probe Atomic Microscopy (KPFM). The Electron Probe Microanalysis (EPMA-JEOL JXA-8530F) was utilised to examine the sample composition & atomic distribution and the elemental mapping.

### S1.2 Gas Sensing and I-V Characteristic Measurement

We performed temperature-dependent I-V measurement (current-voltage) of the sensor with temperature varying from 25 °C to 200 °C, using a DC probe station (Agilent semiconductor devise analyser_SDA, B-1500A, Keysight) with ATT temperature controller.

The whole gas sensing measurement was carried out inside the chamber (in-house developed volumetric setup, vol-29,601 cm$^3$) using two mass flow controllers (MFCs, Alicat Scientific, Inc. USA) of 500 sccm each, temperature controller (Eurotherm) and a data acquisition system. For gas sensing measurement, dry synthetic air (99.99% purity, 80% nitrogen and 20% oxygen) was used as a reference gas and for diluting hydrogen gas (target gas). After stabilising with synthetic air, different concentrations of hydrogen gas were purged by mixing hydrogen gas with synthetic air using a static mixer and the change in current was observed as a gas response. The dynamic change in electrical signal was also measured after purging hydrogen gas by using Keithley SMU 2450 giving a potential of 1V across sensing film.

## S2. Characterization

The average crystallite size was calculated using the Debye-Scherrer relation,[28] considering the most intense diffraction peak of the diffractogram (002). The expression is given as:

$$S = \frac{k\lambda}{\beta \cos\theta} \qquad (S1)$$

The strain (e) was calculated using,

$$\epsilon = \frac{b}{4\tan\theta} \qquad (S2)$$

where S is the crystallite size, K represents the Scherrer constant (0.98), λ denotes the wavelength (1.54Å), β denotes the full width at half maximum (FWHM) and q denotes Bragg's angle. The values estimated are tabulated below:

**Table S1.** Crystallite size and strain value for all fabricated sample.

| Sample | Crystallite Size 'S' (nm) | Strain 'ε' ($\times 10^{-2}$) |
|---|---|---|
| Pristine ZnO | 11.21 | 1.05 |
| Pt_1s-ZnO | 11.62 | 1.01 |
| Pt_2s-ZnO | 11.75 | 0.98 |
| Pt_4s-ZnO | 11.92 | 0.98 |
| Pt_6s-ZnO | 11.86 | 0.98 |

The crystallite size was found to slightly increase because of aggregation of the small crystallites with an increase in the duration of sputtering of Pt over ZnO. On the other hand, strain was reduced with increase in the sputtering time.
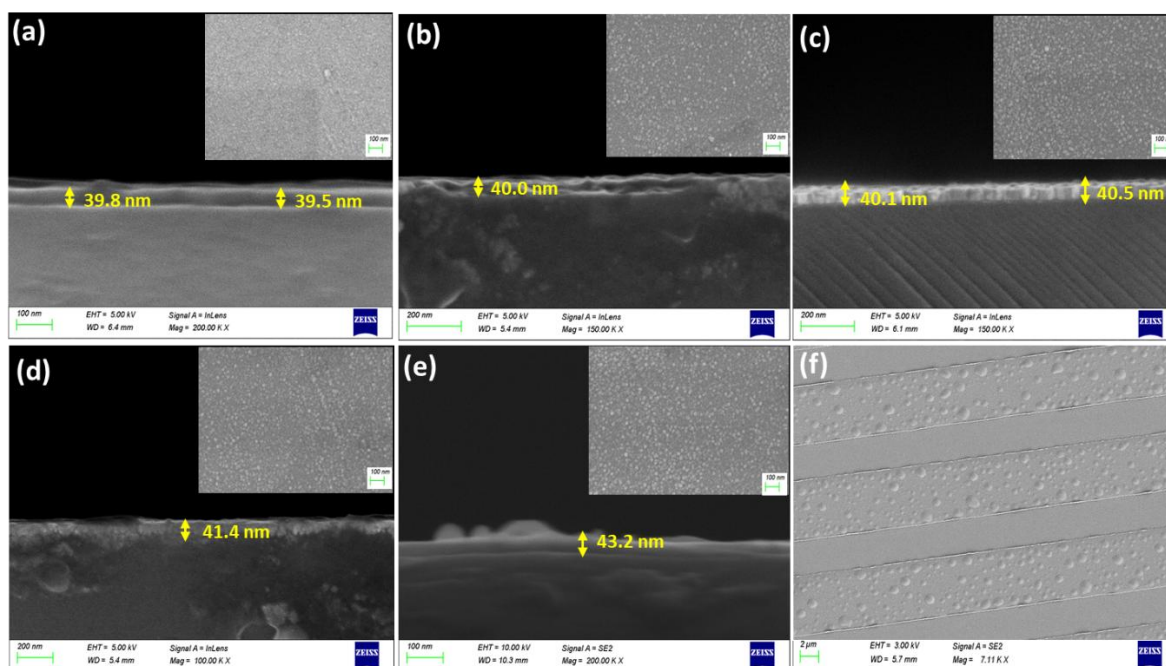
**Figure S1.** Field emission SEM (FESEM) morphology and thickness from cross-sectional imaging of (a) pristine ZnO and Pt decorated ZnO decorated with (b) 1 sec (c) 2 sec (d) 4 sec and (e) 6 sec deposition times. (f) SEM image of uniform coverage of Pt decorated ZnO thin film (at 2 sec deposition time) over the IDE.
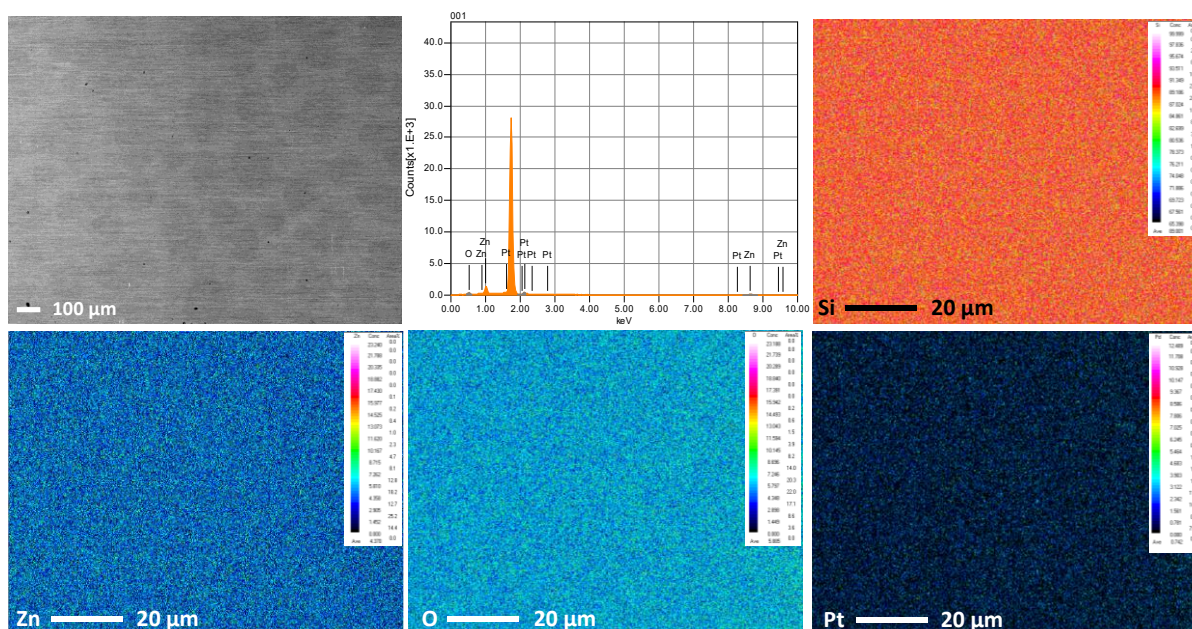


**Figure S2.** Electron probe microanalyzer (EPMA) colour map analysis of Pt (2 sec) decorated ZnO.

**Table S2.** EPMA point analysis indicating atom and mass percentages of O, Zn and Pt in pristine ZnO and Pt decorated ZnO with 1, 2, 4 and 6 sec deposition times.

| Sample | Atom% | | | Mass% | | |
|---|---|---|---|---|---|---|
| | O | Zn | Pt | O | Zn | Pt |
| ZnO | 45.92 | 54.08 | - | 17.90 | 82.10 | - |
| Pt_1s-ZnO | 57.68 | 42.07 | 0.25 | 24.80 | 73.90 | 1.30 |
| Pt_2s-ZnO | 58.09 | 41.42 | 0.49 | 24.90 | 72.53 | 2.57 |
| Pt_4s-ZnO | 53.23 | 45.30 | 1.47 | 20.77 | 72.24 | 6.99 |
| Pt_6s-ZnO | 57.20 | 39.72 | 3.08 | 22.25 | 63.13 | 14.62 |

**Table S3**. Binding energy (in eV) and relative percentages of $O_{lat}$ and $O_{ads}$ species on pristine and Pt decorated ZnO films.

| Sample | Oxygen Species | Binding Energy (eV) | Relative Percentage (%) |
|---|---|---|---|
| ZnO | $O_{lat}$ | 530.7 | 72.15 |
| | $O_{ads}$ | 532.4 | 27.84 |
| Pt_1s-ZnO | $O_{lat}$ | 530.4 | 28.84 |
| | $O_{ads}$ | 531.6 | 71.16 |
| Pt_2s-ZnO | $O_{lat}$ | 530.0 | 27.47 |
| | $O_{ads}$ | 531.1 | 72.52 |
| Pt_4s-ZnO | $O_{lat}$ | 530.1 | 20.89 |
| | $O_{ads}$ | 531.8 | 79.50 |
| Pt_6s-ZnO | $O_{lat}$ | 530.0 | 15.87 |
| | $O_{ads}$ | 531.6 | 84.12 |
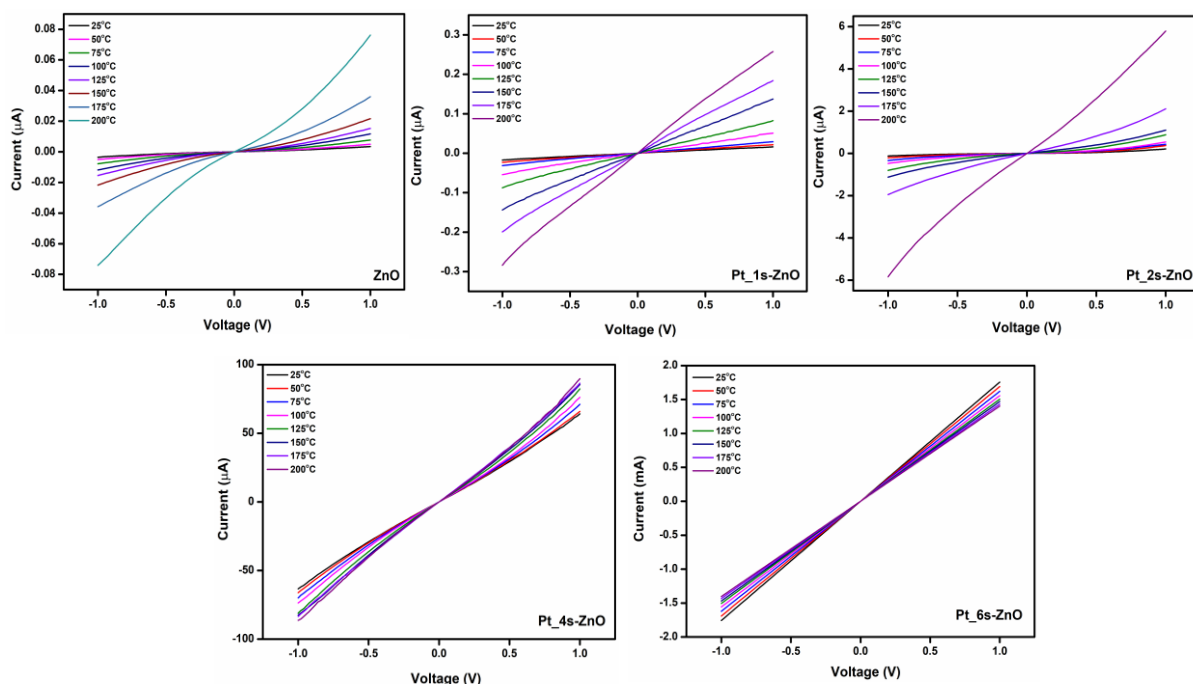
**Figure S3.** Current-voltage (I-V) characteristics of (a) pristine ZnO and Pt decorated ZnO with Pt deposition time of (b) 1 sec, (c) 2 sec, (d) 4 sec and (e) 6 sec. We examined the resistivity of the interdigitated electrodes (IDEs) by varying the temperature from 25 °C to 200 °C.
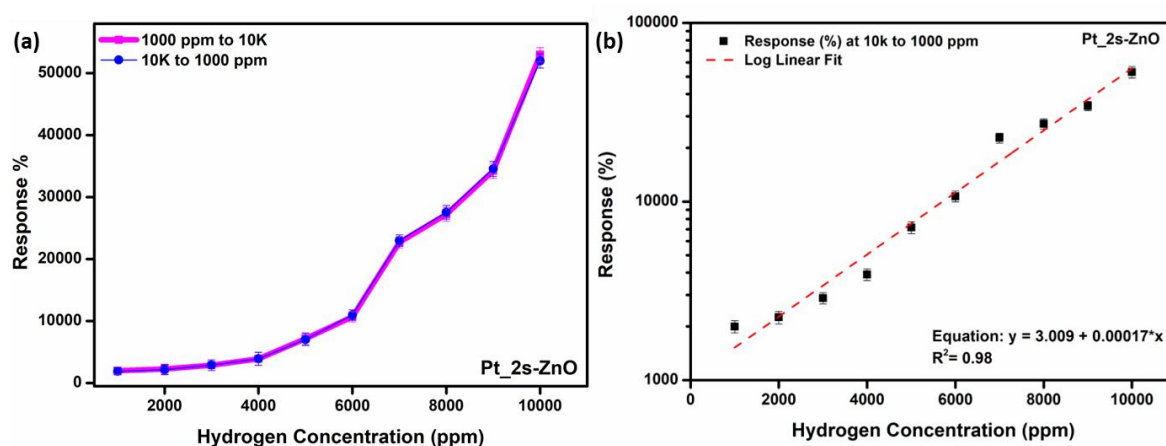


**Figure S4.** (a) The response % as a function of hydrogen concentration, representing hysteresis for Pt decorated (deposition time 2s) ZnO sample and (b) Linearity in the response of the sensor as a function of higher concentration (1000 to 10k ppm) of hydrogen concentration.

**Table S4.** Quantitative sensor response values toward hydrogen and other interfering gases (5 ppm) at 225 °C.

| Different Gases | Sensitivity of Pt-ZnO | Sensitivity of Only ZnO |
|:---:|:---:|:---:|
| Hydrogen | 185% | 5% |
| CO | 20% | 25% |

| | | |
|---|---|---|
| Ammonia | 40% | 60% |
| Ethylene | 30% | 50% |
| Methane | 10% | 14% |
| NO$_2$ | 2% | 3% |
| Acetone | 5% | 14% |

## S3. Work function calculations

The work function of the fabricated sample was calculated after being calibrated with highly oriented pyrolytic graphite (HOPG) with a known work function as a benchmark to ensure the precision of our Kelvin probe force microscopy (KPFM) measurement. The work function of the sample can be measured by **Equation S3**.

$$\emptyset_s = \emptyset_t - eV_{CPD} \qquad\qquad (S3)$$

here, $\emptyset_S$: Work function of the sample

$\emptyset_t$: Work function of the tip

'e' signifies the charge of a single electron

$V_{CPD}$: Contact Potential Difference between the probe tip and sample surface

## S4. Comparison with literature

**Table S5:** Comparation of Sensing result with other Literature

| Sl No. | Sensing Materials | Technique/ Preparation | Response and Recovery time | OT (ºC) | Hydrogen Conc (ppm) | Sensing Response | Ref |
|---|---|---|---|---|---|---|---|
| 1 | Pd doped ZnO nanorods | Sol-gel synthesis | 75/441 sec | RT | 360 ppm | 1302% | 14 |
| 2 | Pd doped ZnO/SnO$_2$ | Electrospun precursor | 20/6 sec | 120ºC | 100 ppm | 160 | 17 |
| 3 | On-chip growth of ZnO with PdO decoration | Hydrothermally grown ZnO decorated with PdO by sputtering. | - | 350ºC | 500 | 3.6 | 26 |
| 4 | Sb doped ZnO | Spray pyrolysis system | 100-350/600-800 sec | 250ºC | 10 ppm | 23 | 16 |

| | | | | | | | |
|---|---|---|---|---|---|---|---|
| 5 | ZnO:Ag nanowire | Electrochemical deposition | 22/11 sec | RT | 100 ppm | 50 | 13 |
| 6 | Ni-doped ZnO | Ni chips were attached with the ZnO target | - | 150ºC | 10,000 ppm 5 ppm | 69% 17.77% | 23 |
| 7 | Pd-ZnO nanosheets | Hydrothermal method, and Pd-decoration using UV irradiation | 336/294 sec | 250ºC | 50 ppm | 2.514 | 19 |
| 8 | $In_2O_3$ doped Pd@ZnO | Facile hydrothermal approach | 0.4 and 4.0 min | 300ºC | 100 ppm | 42 | 10 |
| 9 | Co-ZnO N/C | Chemical synthesis | 26/17 sec | RT | 1% ppm | 3.7% | 9 |
| 10 | Mg doped ZnO | RF sputtering with $Mg_{0.2}Zn_{0.8}O$ target | 75/54 sec | RT | 700 ppm | 70 | 29 |
| 11 | N-doped ZnO | Chemical synthesis | 23 sec | 200 °C | 100 ppm | 73% | 65 |
| 12 | Al/Ga Co-doped ZnO | Sol-gel grown | 10/8 min | 100ºC | 250 ppm | 60% | 66 |
| 13 | AuNs@ZnO | Sputtering followed by heat treatment | - | 400◦C | 75 ppm | 21% | 25 |
| 14 | Al-doped ZnO | Mather-type plasma focus device using Al content ZnO target. | - | 300◦C | 1000 ppm 100 ppm | 66% 17% | 67 |
| 15 | Pt decorated ZnO | DC reactive sputtering with annealed at 600 °C. | - | 300ºC | 75 ppm | 60% | 24 |
| 16 | 3% Cu-doped ZnO | Pulsed laser deposition technique. | 65/250 sec | 150ºC | 1000 ppm | 51% | 68 |
| 17 | W doped ZnO | Co-sputtering technique | - | 150ºC | 100 ppm | 67% | 69 |
| 18 | rGO-decorated Ni-doped ZnO | Sputtering and Chemical synthesis process | 28 sec | 150º | 100 | 63.8% | 70 |
| **19** | **Pt decorated ZnO** | **2 sec Sputtering of Pt over ZnO thin film** | **10/3 sec** | **225ºC** | **0.1 ppm** | **38%** | **Our Work** |

## S5. Computational details

### S5.1 Pseudo molecule calculations

To cancel the dipole and achieve swift convergence in density functional theory (DFT) calculations, we cap one of the surfaces of the (002) slab with pseudo hydrogens of appropriate nuclear charge to replicate the missing Zn or O bonds. Electron counting rules determine the choice of capping charge. In the case of wurtzite ZnO, the bulk coordination number is 4. Each oxygen contributes 6 electrons to 4 bonds, effectively 1.5 electrons per bond. Each zinc contributes 2 electrons to 4 bonds, effectively 0.5 electrons per bond. Thus, one unsaturated bond for an oxygen atom needs to be compensated by the equivalent nuclear charge of a missing Zn atom that should have contributed 0.5 electrons to that bond, i.e., with a pseudo-hydrogen of charge +0.5. Similarly, one unsaturated bond for a zinc atom must be compensated with a pseudo-hydrogen of charge +1.5.

Apart from the core charge on the pseudo-hydrogen, we also calculate the optimal bond distances for O or Zn with pseudo-hydrogens by considering pseudo-molecules. Specifically, we consider $Zn(Hn)_4$ and $O(Hn)_4$ molecules, where $n$ is the nuclear charge, relax the bond distances of these molecules using DFT to get the optimum bond distance, and initialize the pseudo-hydrogens at these optimized bond distances within slab models. Within each pseudo-molecule, we initialized the bonds in a tetrahedral fashion, similar to the coordination environment within bulk ZnO. The optimized bond distances are listed in **Table S6**.
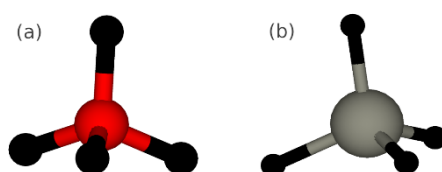


**Figure S5.** Optimised structures of pseudomolecules (a) $O(H_{0.5})_4$ and (b) $Zn(H_{1.5})_4$. Red, grey and black spheres are oxygen, zinc and pseudo-hydrogens, respectively.

**Table S6.** Optimised bond lengths of the pseudomolecules. All molecules are initialised in a tetrahedral coordination.

| Pseudo molecule | Bond length ( Å ) |
|:---:|:---:|
| $O(H_{0.5})_4$ | 1.03 |
| $O(H_{1.5})_4$ | 1.63 |
| $Zn(H_{1.5})_4$ | 1.58 |

**S5.2 Absolute surface energies:**

The two terminations $t_1$ and $t_2$ of the (002) plane are capped with appropriate pseudo-hydrogens and at distances obtained **Table S6**. Once capped, the structure is relaxed with the capping side 'frozen' and only two layers of the exposed surface allowed to relax. The obtain the absolute surface energies of capped surfaces, we used the non-polar (100) surface as the reference, using the following relation:

$$E_{capped}^{100} - E_{uncapped}^{100} = E_{capped}^{002} - E_{uncapped}^{002}$$

In the above relationship, the uncapped energies are the absolute energies. The calculated absolute energies are given in **Table S7**.

**Table S7.** Relative (capped) and absolute (uncapped) surface energies of the $t_1$ and $t_2$ terminations of the (002) surface and the (100) reference. The pseudo-hydrogen atoms used for capping are indicated for each surface energy calculation.

| Surface | Capping | Capped (relative) $E_{surf}$ $(J/m^2)$ | Uncapped (absolute) $E_{surf}$ $(J/m^2)$ |
|:---:|:---:|:---:|:---:|
| (100) | O-$H_{0.5}$, Zn-$H_{1.5}$ | -2.88 | 1.28 |
| (002), $t_1$ | O-$H_{0.5}$ | -2.40 | 1.76 |
| | Zn-$H_{1.5}$ | -2.24 | 1.92 |
| (002), $t_2$ | O-$H_{1.5}$ | 1.44 | 5.76 |
| | Zn-$H_{1.5}$ | 5.28 | 9.61 |

### 5.3 Platinum clusters:

Tetrahedral and planar Pt clusters are placed on the (002) surface. The binding energy of the cluster is calculated according to **Equation 2** of the main manuscript, where adsorbate is the $Pt_4$ cluster.
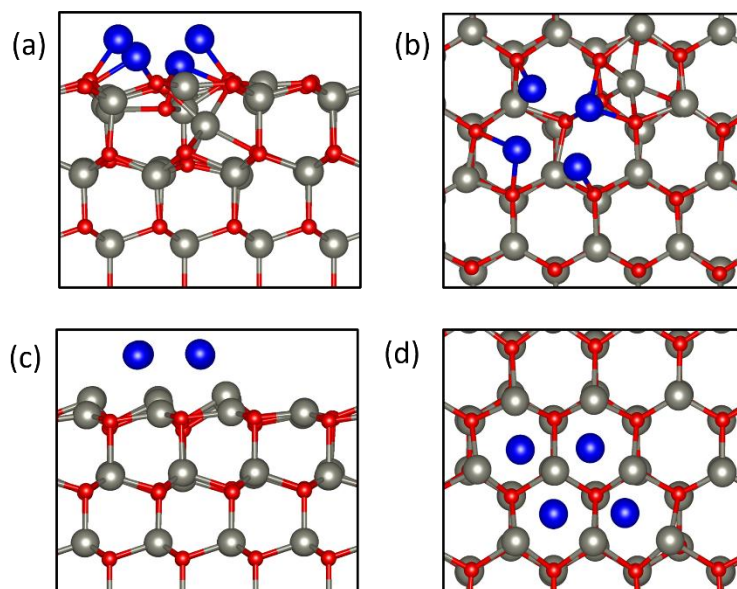


**Figure S6.** Relaxed structures of the best binding $Pt_4$ cluster. (a) and (b) are the side and the top views of the Pt decorated O-$t_1$ surface, while (c) and (d) are the side and the top views of the Pt decorated Zn-$t_1$ surface.

**Table S8.** Binding energies of tetrahedral and planar clusters on both the exposed (002) facets of the $t_1$ termination of ZnO.

| Surface | Termination | Pt$_4$ cluster type | Cluster Binding energy (eV) |
|---------|-------------|---------------------|------------------------------|
| 002 | O-$t_1$ | Tetrahedral | -7.61 |
| | O-$t_1$ | Planar | **-9.76** |
| 002 | Zn-$t_1$ | Tetrahedral | -12.02 |
| | Zn-$t_1$ | Planar | **-12.62** |

All three sites on pristine ZnO were tested for cluster binding. The planar cluster binds best irrespective of the termination, as calculated in **Table S8**. The best binding clusters are the planar cluster initialized over sub-surface Zn for the O-$t_1$ surface with a binding energy of -9.76 eV and the planar cluster initialized on hollow sites of the Zn-$t_1$ surface with a binding energy of -12.62 eV.
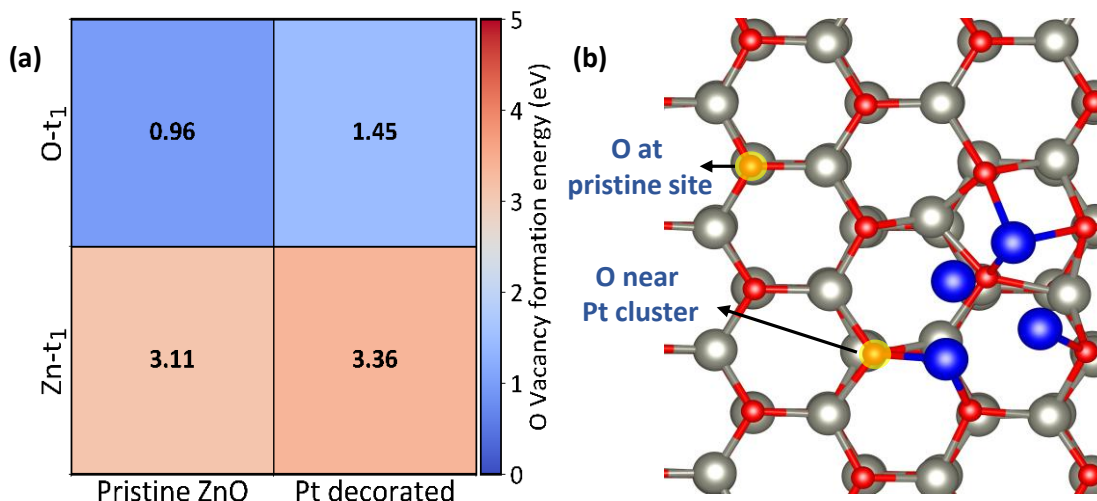


**Figure S7.** (a) Oxygen vacancy formation energy of both the O-$t_1$ and Zn-$t_1$ surfaces. (b) O sites considered in this study. In the Pt decorated slab, we considered the removal of an O atom that lies adjacent to the Pt cluster.
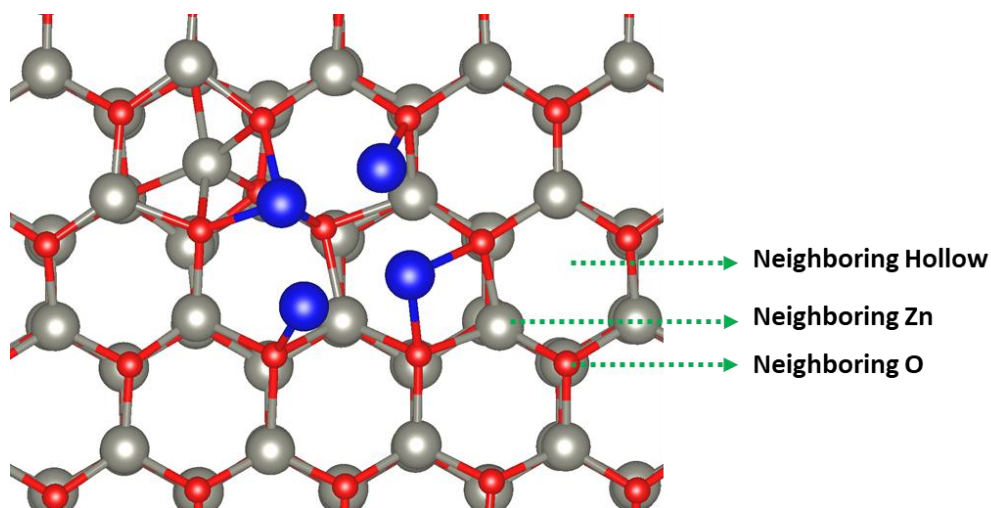


**Figure S8:** Neighboring sites to the Pt cluster considered for adsorption studies to examine the influence of the Pt cluster on site activation toward $H_2$ adsorption.

We do not observe any site activation due the presence of Pt cluster. The increase in binding energy at hollow site is due to formation of Pt-H bonds and not activation of the site itself. A decrease in binding energy was observed at O binding site indicating a possible repulsive interaction.

**Table S9.** Binding energies of the sites neighboring to the Pt cluster for the O-$t_1$ surface.

| Site | Binding energy (eV) |
|---|---|
| on neighboring O | -0.065 |
| on neighboring Zn | -0.126 |
| on neighboring hollow | -0.255 |

**Humidity Effect:**

Humidity interference tests were performed to assess the sensor's stability under realistic operating conditions. The sensor exhibited consistent hydrogen response in both dry and humid environments which demonstrates that moisture has negligible influence on sensing behavior at higher operating temperature such as 225 °C. This is because the adsorbed water molecules desorb rapidly, allowing the formation of reactive oxygen species that is required for hydrogen sensing. The sensor is expected to retain its performance in realistic environments where moisture is present. This characteristic makes it suitable for practical reliable hydrogen monitoring applications. The corresponding results are presented in **Figure S9**, confirming reliable sensor performance under humid conditions.
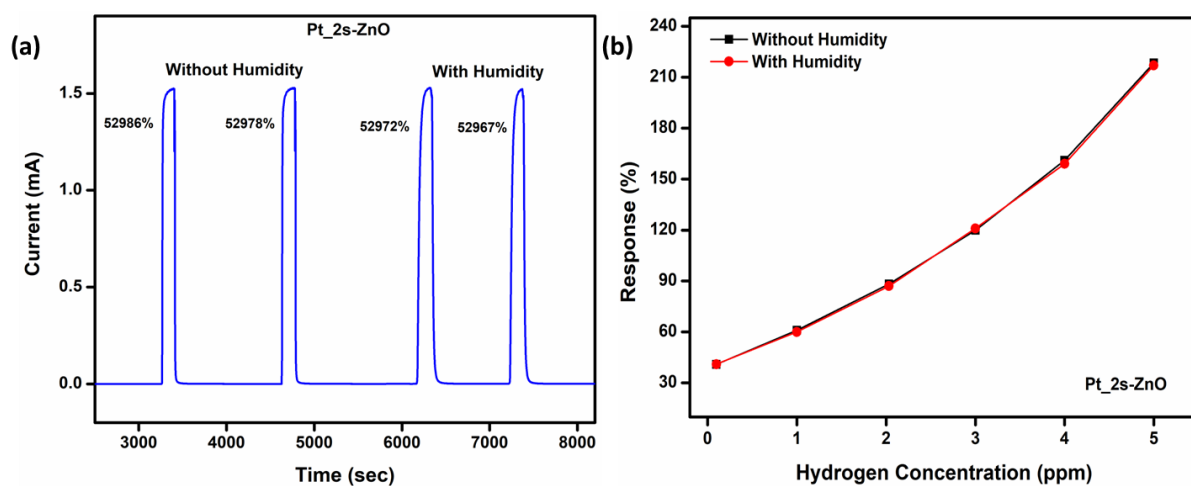
**Figure S9.** Comparison of the sensor response of the Pt nanocluster-decorated ZnO thin film based sensor toward hydrogen under dry and humid environments (a) Towards 10k ppm of Hydrogen gas and (b) lower concentration (5 to 0.1 ppm) of hydrogen gas.